Composite Structures 237 (2020) 111936

Contents lists available at ScienceDirect

Composite Structures

journal homepage: www.elsevier.com/locate/compstruct

Bond behavior of hybrid FRP-to-steel joints

Bo Hu[a,*], Yuan Li[a], Yu-Tian Jiang[a], Huai-Zhong Tang[b]

[a] College of Civil Engineering, Hefei University of Technology, Hefei 230009, PR China
[b] Anhui Chenggu Building Technology Company Limited, Hefei 230000, PR China

ARTICLE INFO

Keywords:
Hybrid FRP
Steel
Bond strength
Effective bond length
Hybrid effect between GFRP and CFRP

ABSTRACT

This paper presents experimental and numerical studies on the bond behavior of hybrid fiber-reinforced polymer (FRP)-to-steel single-lap joints. The hybrid FRP is comprised of inner and outer layers of glass FRP (GFRP) and one intermediate layer of carbon FRP (CFRP). For comparison, the bond behavior of CFRP-to-steel single-lap joints was also examined. Test results show that hybrid FRP-to-steel joints have similar failure modes with three-layered CFRP-to-steel joints. The bond strength of hybrid FRP-to-steel joints is much higher than that of one-layered CFRP-to-steel joints but slightly lower than that of three-layered CFRP-to-steel joints. The effective bond length of hybrid FRP-to-steel joints is close to that of three-layered CFRP-to-steel joints. The numerical investigation indicates that each layer of FRP in the hybrid FRP-to-steel joint undergoes more deformation than the corresponding layer of FRP in the three-layered CFRP-to-steel joint. It confirms that there is a hybrid effect between the inner and outer layers of GFRP and the intermediate layer of CFRP. This is the reason for the effective use of hybrid FRP. Finally, considering the hybrid effect, modified ultimate bond strength and effective bond length models for hybrid FRP-to-steel joints are proposed based on existing modes for CFRP-to-steel joints.

1. Introduction

Externally bonded fiber-reinforced polymer (FRP) has been widely used to strengthen concrete structures for more than two decades. In recent years, the use of externally bonded FRP for strengthening steel structures has attracted significant attention [1–3]. Compared to traditional methods for strengthening steel structures, this technique has obvious advantages, such as a high strength to weight ratio, a lack in residual stress and convenient construction.

Commonly used FRP composites include carbon FRP (CFRP) composites, glass FRP (GFRP) composites, aramid FRP (AFRP) composites and basalt FRP (BFRP) composites. Among these FRP composites, CFRP and GFRP are more widely used than AFRP and BFRP. For the strength enhancement of steel structures, CFRP is preferred rather than GFRP due to its much higher elastic modulus. Recent studies have shown that the use of externally bonded CFRP is very effective for enhancing flexural [4], compressive [5], buckling [6] and fatigue [7,8] behaviors of steel members and structures. However, for outdoor steel structures, such as steel bridges, steel towers and offshore platforms, an issue for strengthening these steel structures by externally bonded CFRP is that carbon is likely to stimulate galvanic corrosion attack on steel when steel is in direct contact with CFRP [9]. Even if there is a resin coating between CFRP and steel, the resin is vulnerable to shrinkage, which may cause cracking of the coating and result in direct contact between CFRP and steel. Furthermore, Tavakkolizadeh et al. [10] experimentally found that the rate of galvanic corrosion significantly decreases with the increase in the epoxy coating thickness but galvanic corrosion still occurs. To prevent galvanic corrosion, a layer of GFRP or a continuous filament polyester drape veil was advised to be installed between CFRP and steel to avoid the direct contact between CFRP and steel [11]. Recently, Alexander [12] designed a multi-layered hybrid FRP composite system, which is comprised of inner and outer layers of GFRP and intermediate layers of CFRP. The inner layer of GFRP acts to protect the steel substrate from potential corrosion due to carbon interaction with steel, while the outer layer of GFRP protects intermediate layers of CFRP against potential wear. Photiou et al. [13] and Sweedan et al. [14] examined the flexural behavior of steel beams strengthened by the hybrid FRP composite system. Test results showed that steel beams strengthened by hybrid FRP reach higher ultimate loads and exhibit ductile responses associated with great deflection. It means that the use of hybrid FRP is also effective to strengthen steel structures despite GFRP has much lower tensile strength and elastic modulus than CFRP. Unfortunately, Photiou et al. [13] and Sweedan et al. [14] did not explain the reason for the effective use of hybrid FRP to strengthen steel structures. The reason should be related to the bond mechanism between hybrid FRP and steel.

* Corresponding author.
E-mail address: bohu@hfut.edu.cn (B. Hu).

https://doi.org/10.1016/j.compstruct.2020.111936
Received 24 May 2019; Received in revised form 31 December 2019; Accepted 13 January 2020
Available online 17 January 2020

For externally bonded FRP-strengthened steel structures, the bond performance between FRP and steel is an important concern. Numerous researchers have investigated the interfacial behavior between CFRP and steel through shear tests of single- [15–23] and double-lap [18,24–35] joints. Five failure modes, including steel-adhesive interface failure [18,25–29,32–34], cohesive failure [15,17,19–22,31,34], CFRP-adhesive interface failure [16,34], CFRP delamination [15–17,19,20,24,25,28,31–34] and CFRP rupture [31,32], have been observed. Test results indicated that the bond strength of CFRP-to-steel joints increases with increases in the total thickness of the CFRP plate/sheets [16,17,32,33], the elastic modulus of the CFRP plate/sheet [17,33] and the thickness of the adhesive [15,17,20,21]. An interesting phenomenon from tests [18,20,24,25,27,29–35] was found that there is an effective bond length beyond which an extension in the bond length cannot improve the bond strength of the joints. It could be concluded that the effective bond length increases as the total thickness of the CFRP plate/sheets increases [30,32]. In addition, it was found that the properties of the adhesive have a significant effect on the bond strength [15,19,28,31,34] and effective bond length [31,34] of the joints. However, so far, limited works have been focused on the performance of multi-layered hybrid FRP-to-steel joints. Hai and Mutsuyoshi [36] examined the structural behavior of pultruded hybrid CFRP/GFRP laminates-to-steel double-lap bolted and bonded-and-bolted joints. Nevertheless, the bond performance of hybrid FRP-to-steel bonded joints has not yet been studied. The reason for the effective use of externally bonded hybrid FRP to strengthen steel structures has not yet been interpreted.

This paper, therefore, presents experimental and numerical studies on the bond behavior of three-layered hybrid FRP-to-steel single-lap bonded joints. The three-layered hybrid FRP is comprised of one inner layer of GFRP sheet, one intermediate layer of CFRP sheet and one outer layer of GFRP sheet. The primary objective of this paper is to reveal the reason for the effective use of hybrid FRP to strengthen steel structures by comparing the bond behavior of three-layered hybrid FRP-to-steel joints with that of one- and three-layered CFRP-to-steel joints. Finally, modified ultimate bond strength and effective bond length models for hybrid FRP-to-steel joints are proposed based on existing models for CFRP-to-steel joints.

2. Experimental program

A total of 36 FRP-to-steel single-lap joints were prepared and tested in tension. The experimental specimens were classified into three groups. The first two groups involved 24 CFRP-to-steel single-lap joints, including 12 specimens with one layer of CFRP and 12 specimens with three layers of CFRP, as shown in Fig. 1 (a) and (b), respectively. The third group concentrated on three-layered hybrid FRP-to-steel single-lap joints, including 12 specimens with inner and outer layers of GFRP and one intermediate layer of CFRP, as shown in Fig. 1 (c). The similar single-lap joint configuration was also used by Fawzia [18].

2.1. Material properties

The steel plates used in this study were hot-rolled Q235 plates with width of 20 mm and thickness of 2.5 mm according to Chinese standard GB/T 700–2006 [37]. Unidirectional CFRP sheets with thickness of 0.167 mm (HM-30, Shanghai Hummer Building Technology Co., Ltd., Shanghai, China) and GFRP sheets with thickness of 0.170 mm (Sika-Wrap-430G, Sika Group, Zurich, Switzerland) were selected for the bond assemblies. A two-component epoxy paste adhesive (Sikadur-30 CN, Sika (China) Ltd., Suzhou, China) was used to bond FRP sheets to steel surfaces. The material properties of the CFRP, GFRP and epoxy adhesive were provided by the manufacturers, while the material properties of the steel plates were obtained through coupon tests in accordance with Chinese standard GB/T228.1-2010 [38]. A summary of the mechanical parameters of these materials are given in Table 1. It should be noted that the ultimate tensile strength values of FRP sheets were for fibers. Although the CFRP sheets, GFRP sheets and epoxy adhesive were provided by different manufacturers, the properties of these materials met the requirements of Chinese code YB/T 4558-2016 [39]. Thus, the compatibility of these materials was satisfied.

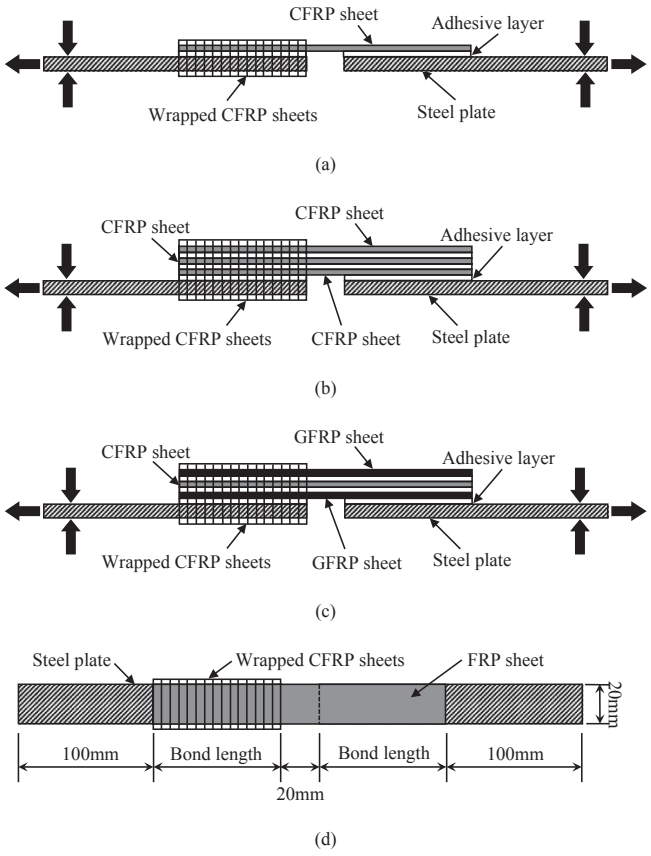

Fig. 1. Schematic view of FRP-to-steel single-lap joints: (a) lateral view of the one-layered CFRP-to-steel joint; (b) lateral view of the three-layered CFRP-to-steel joint; (c) lateral view of the three-layered hybrid FRP-to-steel joint; and (d) front view.

Table 1
Mechanical properties of test materials.

Material	Elastic modulus (GPa)	Elongation at break (%)	Yield strength (MPa)	Ultimate tensile strength (MPa)
Steel plate	203.0	28.5	393	569
CFRP sheet	236.7	1.7	–	3596
GFRP sheet	76.0	2.8	–	2300
Adhesive	4.5	1.5	–	24

2.2. Specimen configuration and preparation

Single-lap joints were adopted in the present study. Fig. 1 shows lateral and front view of the joint specimens. Each specimen was manufactured by bonding two steel plates using FRP sheets and the epoxy adhesive. The FRP attached on each steel plate has the same bond length. The width of the attached FRP was 20 mm. Each specimen had two lap zones between the FRP and the steel plates. One lap zone was the test object and its interfacial failure was expected. The other lap zone was wrapped with three layers of CFRP to ensure its interfacial failure would not happen. The width of the wrapped CFRP was equal to the bond length of the attached FRP. A 20 mm long gap existed between two steel plates to eliminate localized effects such as stress

concentrations on the test interface due to the wrapped CFRP.

Before bonding the joint, two steel plates were polished by a waterproof abrasive paper to remove rust and other contaminants within the bonded surfaces. It should be noted that one steel plate had one bonded surface, while the other had two bonded surfaces because of the additional wrapping process. Before that, a table with a flat top was prepared, on which the positions of the steel plates were marked with rulers and pens. The polished steel plates were placed in the marked positions and fixed on the table top with tapes. This was to ensure the alignment of the specimen in the process of preparation. Then, ethanol was used to further clean the surfaces of the steel plates. After the steel surfaces were fully dry, a thin coating of epoxy adhesive was applied uniformly on the top surfaces of the two steel plates using a brush. Subsequently, a sheet of FRP, which was cut to the required dimension before the bonding process, was attached on the steel plates immediately and pressed uniformly to completely saturate the FRP sheet with the resin and squeeze out the air bubbles in the adhesive layer. Meanwhile, the extruded adhesive was scraped off with a knife. Before attaching the FRP sheet, a steel plate with width of 20 mm, length of 20 mm and thickness of 2.9 mm was placed in the position of the gap to support the FRP sheet and ensure the alignment of the fibers. For three-layered CFRP- and hybrid FRP-to-steel joints, this process was repeated until three layers of FRP had been applied. The specimens were cured for at least 24 h before wrapping three layers of CFRP to ensure that no slippage or damage would occur between FRP sheets and/or between the FRP sheet and the steel surface during the manufacturing process. The same preparation procedure was used for wrapping three layers of CFRP. Finally, the whole specimen was cured at room temperature for at least one week.

Before testing the joint, it was necessary to measure the thickness of the adhesive layer. Firstly, the total thickness of the test lap joint was measured using a vernier caliper. Then, the total adhesive thickness was determined by subtracting the thicknesses of the steel plate and each FRP sheet from the measurement. For three-layered FRP-to-steel joints, it was assumed that the thickness of the adhesive layer between FRP sheets is equal to that of the adhesive layer between the FRP sheet and the steel plate. This assumption was also used by Fawzia et al. [25] and Al-Zubaidy et al. [30]. Consequently, the measured average thickness of the adhesive layer was 0.4 mm for all the specimens in this experimental program.

The identification of the specimens in the experimental program is presented in Table 2. The letters “CF” and “HF” represent the FRP used was CFRP and hybrid FRP, respectively. The numbers “1” and “3” after the letters “CF” represent the CFRP used had one layer and three layers, respectively. The following numbers “20”, “40”, “60” and “80” correspond to the bond lengths. The final numbers “1”, “2” and “3” mean that the same test with the same characteristics was repeated three times.

2.3. Instrumentation and loading procedure

All the specimens were tested in tension using a universal tensile testing machine (WDW-100D) with a maximum capacity of 100 kN. The tensile load applied to the specimens was monotonically imposed with a constant displacement rate of 0.2 mm/min [21]. The test was continued until failure of the specimen. Fig. 2 depicts an overview of the test setup.

2.4. Results and discussion

2.4.1. Failure mode

In this test program, the failure of all the specimens occurs in the lap zones without CFRP wrapping, while the lap zones with CFRP wrapping remain intact after testing. Teng et al. [2] categorized the possible failure modes of FRP-to-steel bonded joints into five modes, including steel-adhesive interface failure (M1), cohesive failure (M2), FRP-adhesive interface failure (M3), FRP delamination (M4) and FRP rupture (M5). In the current experimental program, modes M1, M2 and M4 are observed, while modes M3 and M5 are not found. Note that when some fibers remain on the adhesive and the rest are separated from the adhesive, the failure mode is referred to as FRP delamination [1,15]. Table 2 lists the observed failure modes of all the specimens. Fig. 3 depicts typical photographs of the specimens after the tests. In some specimens (i.e., HF-60-1, HF-60-2 and HF-60-3), steel-adhesive interface failure occurs after the cohesive debonding crack and FRP delamination have propagated over a substantial part of the interface towards the free end of the FRP sheets. Since this interface failure occurs late in the process of cohesive failure and FRP delamination, it is not taken to be the failure mode of these specimens. That is, these specimens are considered to fail by cohesive failure (M2) and FRP delamination (M4).

As shown in Table 2 and Fig. 3, mixed failure occurs in all the specimens. Xia and Teng [15] experimentally found that cohesive failure dominates in FRP-to-steel bonded joints when the thickness of the adhesive layer is less than 2 mm. In the present test program, the measured average thickness of the adhesive layer is 0.4 mm. Hence, cohesive failure (M2) occurs in all the specimens. Some specimens exhibit the debonding of the interface between the steel plate and the adhesive, which is steel-adhesive interface failure (M1). It might be attributed to some misalignment of the specimens during loading. The misalignment leads to some bending in the specimens, which cause the development of vertical peeling stress. The peeling stress results in the debonding of the steel-adhesive interface. However, the observed failure modes reflect the characteristics of the bond strength of the joints well. For three-layered CFRP- and hybrid FRP-to-steel joints, cohesive failure (M2) occurs when the bond length is 20 mm, while both cohesive failure (M2) and FRP delamination (M4) are observed when the bond length exceeds 40 mm. It reveals that the adhesive layer dominates in the load capacities of the joints when the bond length is smaller, while the FRP sheets join in and provide more load capacities for the joints when the bond length is greater. This is also the reason that the bond strength of the joints has a significant enhancement when the bond length increases from 20 mm to 40, 60 and 80 mm. For one-layered CFRP-to-steel joints, both cohesive failure (M2) and FRP delamination (M4) happen. It indicates that the load capacities of one-layered CFRP-to-steel joints with bond lengths of 20, 40, 60 and 80 mm are dominated by both the adhesive layer and the CFRP sheet. The similar failure modes bring almost the same bond strength of the joints.

2.4.2. Bond strength

Table 2 lists the bond strength, P_{exp}, of all the specimens. The average bond strength, $\bar{P}_{exp}$, for the same three joints is employed to highlight the effects of the FRP configuration and the bond length on the bond strength and summarized in Table 2. Corresponding coefficients of variations (COV) are also listed in Table 2. Fig. 4 also shows the comparison of the average bond strength of FRP-to-steel single-lap joints with three FRP configurations and four bond lengths. Note that HF-60-1 suffered damage before testing and its bond strength is not used to estimate the average value.

It can be seen from Table 2 and Fig. 4 that the bond strength of one-layered CFRP-to-steel joints changes little as the bond length increases from 20 mm to 80 mm, whereas the bond strength of three-layered CFRP-to-steel joints has a significant enhancement when the bond length is less than 40 mm and almost does not increase when the bond length exceeds 40 mm. It indicates that the increase in the bond length does not necessarily lead to the improvement of the load capacity of the CFRP-to-steel interface. When the number of CFRP layers increases from one to three, the bond strength of CFRP-to-steel joints with bond lengths of 20, 40, 60 and 80 mm increases by 31%, 76%, 54% and 102%, respectively. It means that the increase in the total thickness of CFRP sheets significantly improves the load capacity of the CFRP-to-steel interface. Similar phenomena were also observed in

Table 2
Experimental, numerical and predicted results.

Specimen	Bond length (mm)	Experimental results					Numerical results				Predicted results			
		P_{exp} (kN)	$\bar{P}_{exp}$ (kN)	COV (%)	$L_{e,exp}$ (mm)	Failure mode	P_{num} (kN)	$\frac{P_{num}}{P_{exp}}$	$L_{e,num}$ (mm)	Y/N[c]	$P_{u,pre}$ (kN)	$\frac{P_{u,pre}}{P_{u,exp}}$	$L_{e,pre}$ (mm)	Y/N[c]
CF1-20-1	20	2.49	2.62	5.6	< 20	M1, M2, M4	2.42	0.92	< 20	Y	2.71	1.03	16.0	Y
CF1-20-2		2.78				M1, M2, M4								
CF1-20-3		2.59				M1, M2, M4								
CF1-40-1	40	2.55	2.56	10.9		M1, M2, M4	2.53	0.99			2.71	1.06		
CF1-40-2		2.85				M1, M2, M4								
CF1-40-3		2.29				M1, M2, M4								
CF1-60-1	60	3.10	2.90	13.2		M1, M2, M4	2.64	0.91			2.71	0.93		
CF1-60-2		2.46				M1, M2, M4								
CF1-60-3		3.14				M1, M2, M4								
CF1-80-1	80	2.15	2.42	12.3		M2, M4	2.64	1.09			2.71	1.12		
CF1-80-2		2.74				M2, M4								
CF1-80-3		2.37				M2, M4								
CF3-20-1	20	3.44	3.44	14.7	20 ~ 30	M1, M2	3.35	0.97	20 ~ 30	Y	–	–	27.8	Y
CF3-20-2		2.94				M1, M2								
CF3-20-3		3.95				M1, M2								
CF3-40-1	40	4.50	4.51	5.3		M2, M4	4.72	1.05			4.69	1.04		
CF3-40-2		4.75				M2, M4								
CF3-40-3		4.27				M2, M4								
CF3-60-1	60	4.16	4.46	6.0		M2, M4	4.94	1.11			4.69	1.05		
CF3-60-2		4.57				M2, M4								
CF3-60-3		4.66				M2, M4								
CF3-80-1	80	5.00	4.88	6.6		M2, M4	5.06	1.04			4.69	0.96		
CF3-80-2		5.12				M2, M4								
CF3-80-3		4.51				M2, M4								
HF-20-1	20	2.82	2.86	1.2	20 ~ 30	M1, M2	2.89	1.01	20 ~ 30	Y	–	–	23.6	Y
HF-20-2		2.89				M1, M2								
HF-20-3		2.86				M1, M2								
HF-40-1	40	4.58	4.37	10.7		M2, M4	4.02	0.92			3.98	0.91		
HF-40-2		3.83				M1, M2, M4								
HF-40-3		4.69				M2, M4								
HF-60-1	60	1.92[a]	3.69[b]	1.1		M2, M4	4.13	1.12			3.98	1.08		
HF-60-2		3.72				M2, M4								
HF-60-3		3.66				M2, M4								
HF-80-1	80	4.26	4.37	4.9		M1, M2, M4	4.21	0.96			3.98	0.91		
HF-80-2		4.62				M1, M2, M4								
HF-80-3		4.24				M1, M2, M4								

Note:
[a] HF-60-1 suffered damage before testing.
[b] The bond strength of HF-60-1 is not used to estimate the average value due to its initial damage.
[c] Y and N represent the numerical or predicted effective bond length agrees and does not agree with the experimental result, respectively.

[16,17,32,33].

Compared to one-layered CFRP-to-steel joints, three-layered hybrid FRP-to-steel joints with bond lengths of 20, 40, 60 and 80 mm have much higher bond strength, increasing by 9%, 71%, 27% and 80%, respectively. It is evident that the additional inner and outer layers of GFRP sheets enhance the load capacity of the joint. The bond strength of three-layered hybrid FRP-to-steel joints has a significant improvement before the bond length achieves 40 mm, but nearly reaches a plateau after the bond length exceeds 40 mm. It is similar to the characteristics of the bond strength of three-layered CFRP-to-steel joints. From three-layered CFRP-to-steel joints to three-layered hybrid FRP-to-steel joints, the inner and outer layers of FRP sheets change from CFRP to GFRP and the bond strength of the specimens with bond lengths of 20, 40, 60 and 80 mm decreases by 17%, 3%, 17% and 10%, respectively. The bond strength of hybrid FRP-to-steel joints is slightly lower than that of three-layered CFRP-to-steel joints. It indicates that there seems to be a possible hybrid effect between the inner and outer layers of GFRP and the intermediate layer of CFRP.

2.4.3. Effective bond length

To determine the effective bond lengths of FRP-to-steel joints with three FRP configurations, trend lines of the average bond strength are plotted against the bond lengths in Fig. 4. Wu et al.'s theoretical analysis [40] showed that the bond strength-bond length curve of a FRP-to-steel pull-pull joint presents a nonlinear relationship. The nonlinear relationship can be represented by a parabolic curve when the bond length is less than the effective bond length, while the relationship becomes a straight line when the bond length exceeds the effective bond length. Accordingly, each average bond strength-bond length trend line consists of a parabolic curve and a straight line for three-layered CFRP-to-steel joints and hybrid FRP-to-steel joints. The straight line was fitted by three data points where the bond lengths are more than 40 mm. Then, the parabolic curve was fitted by two data points where the bond lengths are not more than 40 mm and the slope of the parabolic curve was equal to that of the straight line at the data point where the bond length is 40 mm.

It can be seen that the bond strength of one-layered CFRP-to-steel joints with bond lengths in the range of 20 to 80 mm are almost unchanged. It reveals that the effective bond length of one-layered CFRP-to-steel joints should be less than 20 mm. For three-layered CFRP-to-steel joints, the bond strength has no significant increase after the bond length exceeds a certain value, which is between 20 and 30 mm. This length is the effective bond length of three-layered CFRP-to-steel joints. It should be noted that, although the bond strength still increases after the bond length is beyond the effective bond length, the increase is very slow and then the bond strength is considered to hardly increase in this paper. The effective bond length significantly increases with increasing number of CFRP layers. Similar phenomena were also reported in

Fig. 2. Test setup.

[30,32].

From Fig. 4, it is clear that the bond strength of three-layered hybrid FRP-to-steel joints reaches a steady case after the bond length exceeds a value between 20 and 30 mm, which is defined as the effective bond length of the joints. Compared to one-layered CFRP-to-steel joints, three-layered hybrid FRP-to-steel joints have greater effective bond length. It indicates that three-layered hybrid FRP-to-steel joints need a longer bond length to effectively transfer the stress of the interface between the GFRP sheet and the steel plate and the interface between the GFRP sheet and the CFRP sheet. Interestingly, the effective bond length of three-layered hybrid FRP-to-steel joints is close to that of three-layered CFRP-to-steel joints. The effective bond length seems to be insignificantly influenced by the type of the inner and outer layers of FRP sheets. It might be attributed to the possible hybrid effect between the inner and outer layers of GFRP and the intermediate layer of CFRP.

3. Finite-element modeling

The experimental study in the previous section shows that there is a possible hybrid effect between the inner and outer layers of GFRP and the intermediate layer of CFRP in hybrid FRP-to-steel joints. To further confirm the hybrid effect, three-dimensional finite-element (FE) modeling is conducted using *ABAQUS* software [41] in this section.

3.1. Element types and material models

The test single-lap joints consisted of four different layers, which were CFRP and GFRP sheets, steel plates and adhesive layers. CFRP and GFRP sheets were modelled by eight-node quadrilateral in-plane general-purpose continuum shell elements (SC8R). This type of element, which is capable of predicting FRP failure, has been successfully utilized to simulate FRP composites by Al-Zubaidy et al. [32]. The stress-strain relationships of CFRP and GFRP sheets were idealized to be linear-elastic up to failure, as shown in Fig. 5(a). The elastic modulus, E_f, and ultimate tensile strength, f_{fu}, which were provided by the manufacturers and are listed in Table 1, were used to determine the ultimate strain, ε_{fu}, and the stress-strain curves of CFRP and GFRP sheets. Eight-node linear brick, reduced integration, hourglass control elements (C3D8R) were selected to model the steel plates. Although the steel plates did not yield in the tests, the classic bilinear kinematic hardening with a post-yield strain hardening of 1% ($E_{sp} = 0.01E_{se}$) was still used to represent the stress-strain relationship of the steel plates, where E_{se} and E_{sp} are the elastic and plastic modulus of the steel plates, respectively, as shown in Fig. 5(b). The elastic modulus, E_{se}, yield strength, f_{sy}, and ultimate tensile strength, f_{su}, of the steel plates were defined according to coupon test results, which are listed in Table 1. Correspondingly, the yield strain, ε_{sy}, and ultimate strain, ε_{su}, were easily determined. For the adhesive layers, eight-node cohesive elements (COH3D8) were used. The traction-separation laws were employed to simulate the stress-displacement relationships of the adhesive layers in normal and shear directions, as shown in Fig. 5(c). The separation is a location change in the normal or shear direction between upper and lower nodes of a cohesive element during loading. The peak traction in the normal direction, T_n^0, was taken as 24 MPa, which is the ultimate tensile strength value in Table 1. The peak traction in the shear direction, T_s^0, was taken as 10 MPa, which is the shear strength value of a steel-to-steel single-lap adhesively boned joint and was provided by the manufacturer. It was found that the separations at the peak tractions in normal and shear directions, δ_n^0 and δ_s^0, have little effect on the results. Thus, both δ_n^0 and δ_s^0 were assumed to be 0.005. After trial, the ultimate separations in normal and shear directions, δ_n^u and δ_s^u, were set as 0.04 and 0.1 mm, respectively, which could lead to better predictions. *ABAQUS* software provides several approaches to create the interaction between the FRP sheet and the adhesive layer and the interaction between the steel plate and the adhesive layer, such as surface-to-surface contact, coupling constraints, multi-point constraints and tie constraints [41]. The main intention of the FE modeling in the current study was to investigate the hybrid effect between CFRP and GFRP. Moreover, in the tests, FRP-adhesive interface failure did not happen. Although steel-adhesive interface failure occurred in some of the test specimens, the failure did not dominate. Hence, there was no specific element assigned at the interface between the FRP sheet and the adhesive layer and the interface between the steel plate and the adhesive layer. Tie constraints were used to model FRP-adhesive and steel-adhesive interfaces. The nodes on the interfaces were tied to have equal displacement.

3.2. Geometry, mesh and boundary conditions

Since all the lap zones wrapped by three layers of CFRP did not failed in the tests, only the lap zone without CFRP wrapping was simulated for each joint. Due to material and geometry symmetry, only one fourth of the full-scale joint was modelled. Then, symmetric boundary constraints were applied to the nodes on the planes of symmetry. For symmetric boundary constraints along X-axis, the displacement in the X-axis direction and the rotations around the Y-axis and Z-axis directions of the nodes on the plane of symmetry were constrained. For symmetric boundary constraints along Z-axis, the displacement in the Z-axis direction and the rotations around the X-axis and Y-axis directions of the nodes on the plane of symmetry were constrained. The FE model is depicted in Fig. 6. As shown in Fig. 6, the joint model was divided into three parts: part A, part B and part C. Part A contained FRP sheets and adhesive layers, where the interfacial failure occurred in the tests. During loading, small bending would be induced due to some misalignment of the joint. Because of constant bending and membrane strain approximations of SC8R, high mesh refinement was required to capture bending deformation [41]. Thus, a meshing size of 1 mm was used for part A to obtain accurate simulation results. Meanwhile, to save the computational time, the meshing sizes were taken as 2 and 5 mm for part B and part C, respectively. It should be noted that all the

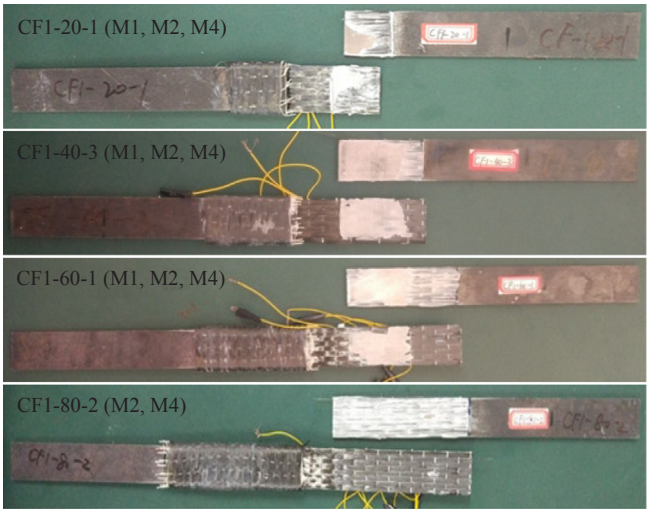

(a)

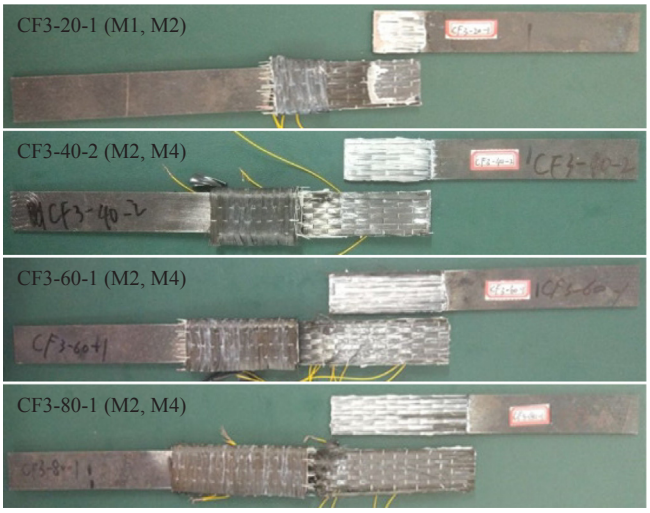

(b)

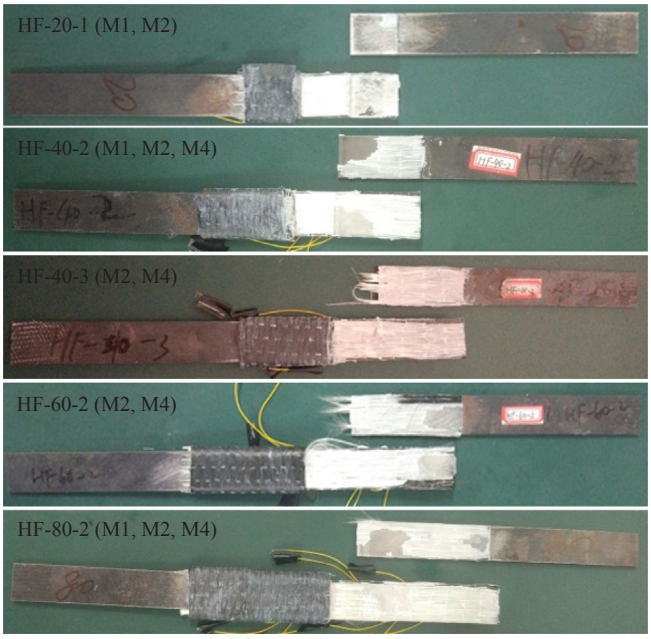

(c)

Fig. 3. Typical failure modes of the specimens: (a) one-layered CFRP-to-steel joints; (b) three-layered CFRP-to-steel joints; and (c) three-layered hybrid FRP-to-steel joints.

meshing sizes were determined after trial. Before the simulation was run, the nodes of part C were restrained against all the displacements in two directions except for the displacement in the direction of the applied load. The load was applied using displacement control. Displacement in the direction of X-axis was applied as a boundary condition to part C.

3.3. Model validation

Table 2 lists the numerical bond strength, P_{num}, of one- and three-layered CFRP-to-steel joints and three-layered hybrid FRP-to-steel joints. Fig. 4 also shows trend lines of numerical bond strength versus bond length relationships. According to the trend lines, the numerical effective bond lengths, $L_{e,num}$, were determined and are listed in Table 2. As shown in Table 2, the ratios, $P_{num}/\bar{P}_{exp}$, are in the range of 0.91 to 1.12. It indicates that the numerical bond strength is in good agreement with the experimental bond strength. Table 2 shows that the numerical effective bond lengths are the same as the experimental effective bond lengths. It can be inferred that the developed FE model predicts the experimental effective bond lengths well. From Fig. 4, it can be seen that the numerical trend lines of bond strength versus bond length relationships agree well with the experimental trend lines. Therefore, the developed FE model simulates the bond behavior of FRP-to-steel single-lap joints well and can be used for the further numerical investigation.

3.4. Numerical investigation on the hybrid effect between GFRP and CFRP

Fig. 7 presents the comparison of numerical FRP longitudinal strain distribution along the bond length between CF3-80 and HF-80. The comparison is made at five load levels. It is obvious that CF3-80 and HF-80 have similar FRP longitudinal strain distribution. The FRP

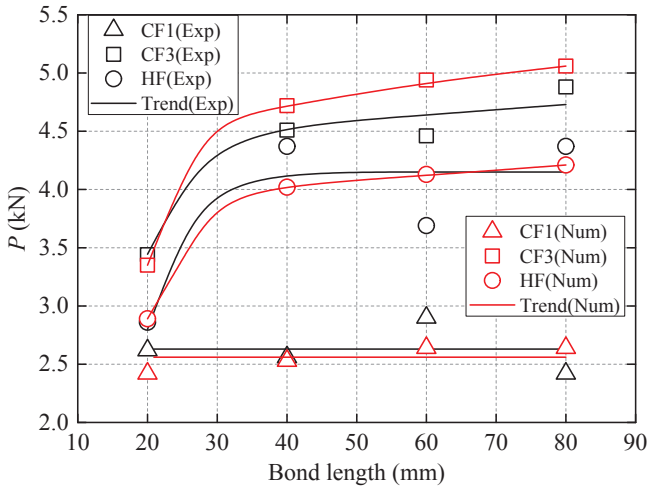

Fig. 4. Experimental and numerical bond strength versus bond length relationships.

longitudinal strain reaches the maximum value at the center of the joint and reduces sharply away from the center of the joint. After the distance away from the center of the joint is beyond the effective bond length, the FRP longitudinal strain decreases slowly. It is also clear that CF3-80 and HF-80 have similar effective bond lengths, which are between 20 and 30 mm. This numerical observation is consistent with the experimental observation. It can be seen from Fig. 7 that, when the load

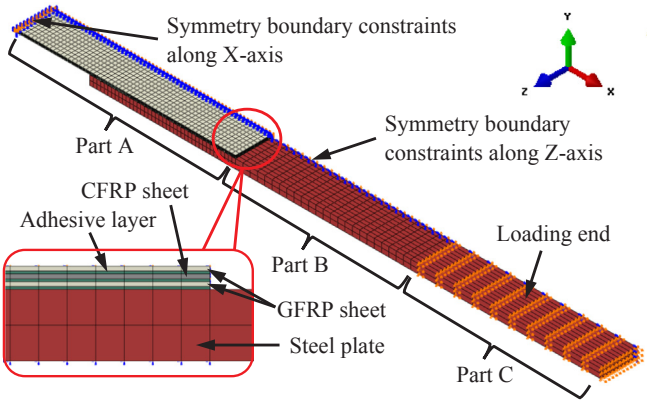

Fig. 6. FE model.

level is very small (0.10*P*), the longitudinal strain of each layer of FRP in HF-80 is slightly lower than that of the corresponding layer of FRP in CF3-80. After the load level exceeds 0.25*P*, the longitudinal strain of each layer of FRP in HF-80 increases faster and is higher than that of the corresponding layer of FRP in CF3-80. The closer the location is to the center of the joint, the greater the strain increases. When the load level achieves 1.00*P*, although the FRP longitudinal strain away from the center of the joint in CF3-80 exceeds that in HF-80, the FRP longitudinal strain near the center of the joint in HF-80 is still higher than that in CF3-80.

The comparison of numerical FRP longitudinal strain distribution

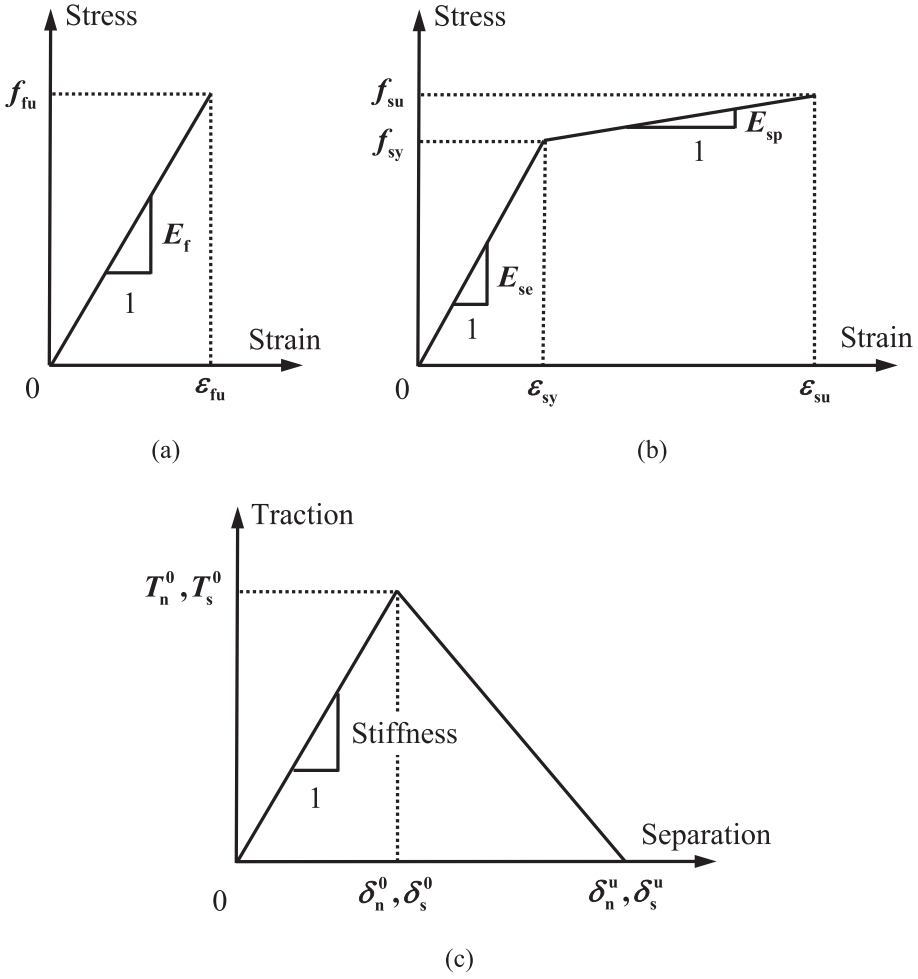

Fig. 5. Material constitutive models: (a) CFRP and GFRP sheets; (b) steel plate; and (c) adhesive layer.

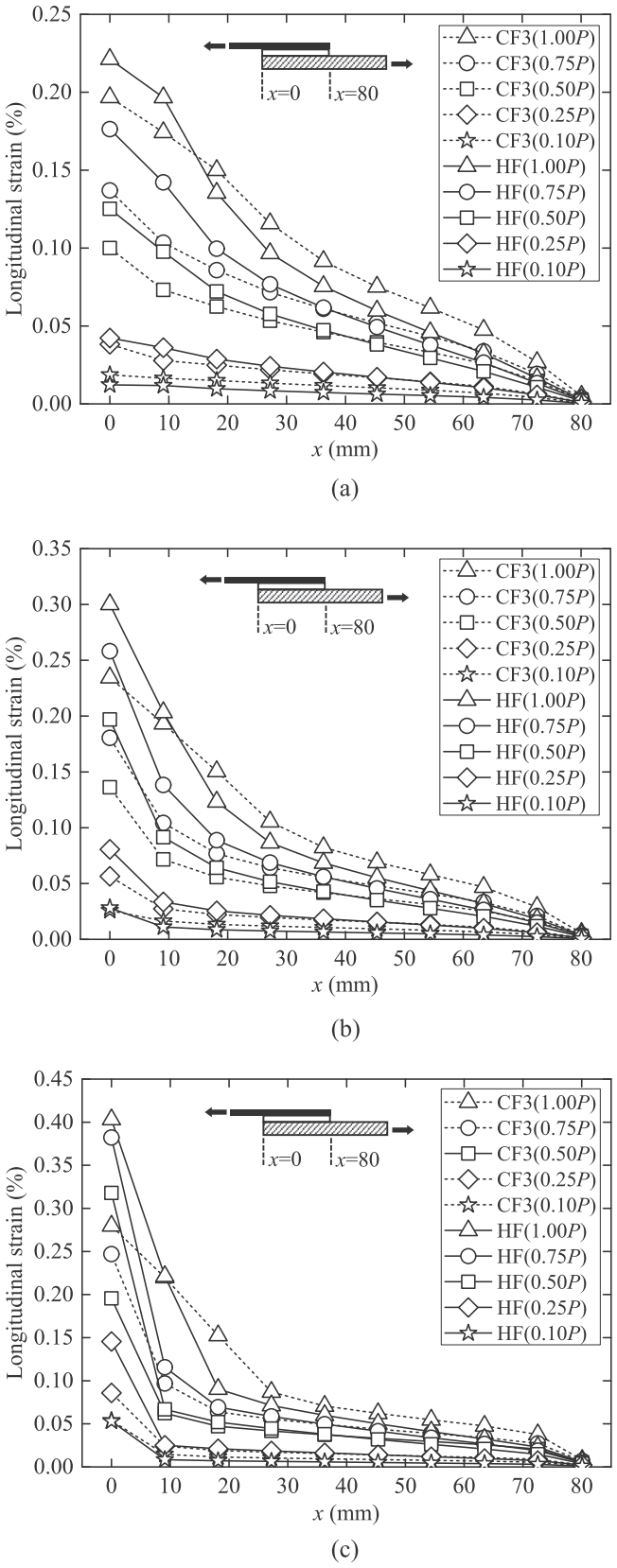

Fig. 7. Comparison of numerical FRP longitudinal strain distribution between CF3-80 and HF-80: (a) outer layers of CFRP and GFRP; (b) intermediate layers of CFRP; and (c) inner layers of CFRP and GFRP.

indicates that the inner and outer layers of GFRP and the intermediate layer of CFRP in the three-layered hybrid FRP-to-steel joint undergo greater deformation than the corresponding layers of CFRP in the three-layered CFRP-to-steel joint during loading. It is clear that there is a hybrid effect between the inner and outer layers of GFRP and the intermediate layer of CFRP. The hybrid effect leads to greater deformation of GFRP and CFRP. Consequently, the bond strength of three-layered hybrid FRP-to-steel joints is slightly lower than that of three-layered CFRP-to-steel joints and the effective bond length of three-layered hybrid FRP-to-steel joints is close to that of three-layered CFRP-to-steel joints. The hybrid effect should be the reason for the effective use of hybrid FRP to strengthen steel structures.

4. Ultimate bond strength and effective bond length models for hybrid FRP-to-steel joints

This section presents modified models to predict ultimate bond strength and effective bond length of hybrid FRP-to-steel joints. The modified models are based on existing ultimate bond strength and effective bond length models for CFRP-to-steel joints. The hybrid effect between GFRP and CFRP is considered in the model modification.

4.1. Existing ultimate bond strength and effective bond length models for CFRP-to-steel joints

The ultimate bond strength model proposed by Wu et al. [40] and the effective bond length model in Chinese code YB/T 4558-2016 [39], which are for CFRP-to-steel Joints, are employed in this section. It should be noted that the bond strength is defined as the ultimate bond strength when the bond length is not less than the effective bond length.

In 2002, Wu et al. [40] conducted a theoretical analysis to solve the nonlinear interfacial stress transfer and fracture propagation problems for different kinds of adhesive joints in FRP/steel-strengthened concrete or steel structures. They proposed a fracture mechanics-based model to estimate the ultimate bond strength, P_u, of the pull-pull single-lap joint:

$$P_u = b_f \sqrt{2E_f t_f G_f} \tag{1}$$

where b_f, E_f and t_f are the width, elastic modulus and total thickness of the FRP, respectively; and G_f is the interfacial fracture energy. The interfacial fracture energy, G_f, was not solved by Wu et al. [40] and can be determined using Bocciarelli et al.'s theoretical solution [26], which was derived through an inverse analysis approach and is given by

$$G_f = \tau_f^2 \frac{t_a e}{G_a} \tag{2}$$

where e is Euler's number ($\approx$2.71828); t_a is the thickness of the adhesive; and τ_f and G_a are the maximum shear strength and shear modulus of the adhesive, respectively, and can be obtained by the following equations:

$$\tau_f = 0.8 f_{t,a} \tag{3}$$

$$G_a = \frac{E_a}{2(1+\mu)} \tag{4}$$

where $f_{t,a}$ and E_a are the ultimate tensile strength and elastic modulus of the adhesive, respectively; and μ is Poisson's ratio of the adhesive and can be assumed to be 0.3.

Based on interfacial fracture mechanics, Chinese code YB/T 4558-2016 [39] specifies a design equation to estimate the effective bond length, L_e, of the FRP-to-steel interface as follow

$$L_e = 19 \frac{f_{t,a}}{E_a} \sqrt{E_f t_f \sqrt{t_a}} \tag{5}$$

where the unit of $f_{t,a}$ is MPa; the units of E_a and E_f are MPa; and the units of t_f and t_a are mm.

Table 2 lists the predicted ultimate bond strength, $P_{u,pre}$, of Wu

et al.'s model [40] and the predicted effective bond lengths, $L_{e,pre}$, of the design model in Chinese code YB/T 4558-2016 [39] for one- and three-layered CFRP-to-steel single-lap joints. It should be noted that the experimental average bond strength, $\bar{P}_{exp}$, is the experimental average ultimate bond strength, $\bar{P}_{u,exp}$, when the bond length is more than the experimental effective bond length, $L_{e,exp}$. In Table 2, the ratios, $P_{u,pre}/\bar{P}_{u,exp}$, are in the range of 0.93 to 1.12. It indicates that Wu et al.'s model [40] predicts the experimental ultimate bond strength of one- and three-layered CFRP-to-steel single-lap joints well. In Table 2, the predicted effective bond lengths of the design model in Chinese code YB/T 4558-2016 [39] are 16.0 and 27.8 mm for one- and three-layered CFRP-to-steel single-lap joints, respectively, which are in good agreement with the experimental results. Therefore, Wu et al.'s model [40] and the design model in Chinese code YB/T 4558-2016 [39] can be used to predict the ultimate bond strength and effective bond lengths of CFRP-to-steel joints in the test program, respectively.

4.2. Model modification considering the hybrid effect between GFRP and CFRP

Experimental and numerical results reveal that there is a hybrid effect between the inner and outer layers of GFRP and the intermediate layer of CFRP. Due to the hybrid effect, the ultimate bond strength of three-layered hybrid FRP-to-steel joints is slightly lower than that of three-layered CFRP-to-steel joints and the effective bond lengths of three-layered hybrid FRP-to-steel joints are close to those of three-layered CFRP-to-steel joints. To take into account the influence of the hybrid effect on the ultimate bond strength and effective bond lengths of hybrid FRP-to-steel joints, a modified equation is proposed for the axial stiffness of the hybrid FRP, $E_f t_f$, as follow

$$E_f t_f = E_{cf} t_{cf} + \alpha E_{gf} t_{gf} \tag{6}$$

where E_{cf} and t_{cf} are the elastic modulus and thickness of the intermediate layer of CFRP, respectively; E_{gf} and t_{gf} are the elastic modulus and total thickness of the inner and outer layers of GFRP, respectively; and α is the hybrid effect coefficient and can be defined as

$$\alpha = \left(\frac{E_{gf}}{E_{cf}}\right)^{\beta} \tag{7}$$

where β is a constant to be determined. One benefit of the form of Eq. (7) is that the hybrid effect between the inner and outer layers of GFRP and the intermediate layer of CFRP is considered. The other benefit is that α is equal to 1.0 when each layer of FRP has the same type.

To determine the constant, β, a database that contains 24 numerical results of three-layered hybrid FRP-to-steel single-lap joints was established. The developed FE model was used to obtain the numerical results. The numerical specimens were classified into six groups. Each group involved 4 specimens with bond lengths of 20, 40, 60 and 80 mm, respectively. The types of GFRP and CFRP sheets used in the test program were employed as the basic types. Additionally, three types of GFRP sheets and two types of CFRP sheets from open literature [32,42–45] were collected for this analysis and are listed in Table 3. With regard to the identification of the numerical specimens, the letters "HF" represent the hybrid FRP. The letters "a", "b" and "c" represent the properties of the inner and outer layers of GFRP were from [42], [43] and [44], respectively. The letters "d" and "e" represent the properties of the intermediate layer of CFRP were from [45] and [32], respectively. The following numbers "20", "40", "60" and "80" correspond to the bond lengths. Table 3 lists the numerical bond strength, P_{num}, of the specimens. Fig. 8 depicts trend lines of numerical bond strength versus bond length relationships. The trend lines were fitted with the same method as described in Section 2.4.3. Based on the trend lines, the numerical effective bond lengths, $L_{e,num}$, can be determined and are listed in Table 3.

According to Eq. (1) and the numerical ultimate bond strength in Table 3, the axial stiffness of the hybrid FRP can be back-calculated by the following equation:

$$E_f t_f = \frac{P_u^2}{2b_f^2 G_f} \tag{8}$$

It should be noted that the numerical bond strength, P_{num}, is the numerical ultimate bond strength, $P_{u,num}$, when the bond length is more than the numerical effective bond length, $L_{e,num}$.

Through a regression analysis of the axial stiffness of the hybrid FRP back-calculated from 18 numerical ultimate bond strength results in Table 3, the constant, β, was determined as shown in Fig. 9 and Eq. (7) is written as

$$\alpha = \left(\frac{E_{gf}}{E_{cf}}\right)^{-0.51} \tag{9}$$

Substituting Eq. (9) into Eq. (6), the axial stiffness of the hybrid FRP, $E_f t_f$, can be determined. Fig. 10 shows the comparison between $E_f t_f$ calculated by Eq. (6) and $E_f t_f$ back-calculated by Eq. (8). It is clear that a good agreement is achieved. It should be noted that Eq. (9) is applicable when the axial stiffness of the inner and outer layers of GFRP, $E_{gf} t_{gf}$, is in the range of 15.36 to 39.42 GPa·mm and the axial stiffness of the intermediate layer of CFRP, $E_{cf} t_{cf}$, is in the range of 27.97 to 39.53 GPa·mm.

4.3. Verification of modified models for hybrid FRP-to-steel joints

Three experimental ultimate bond strength results in Table 2 and 18 numerical ultimate bond strength results in Table 3 were used to verify the modification for Wu et al.'s model [40], while one experimental effective bond length result in Table 2 and 6 numerical effective bond length results in Table 3 were used to validate the modification for the design model in Chinese code YB/T 4558-2016 [39]. Tables 2 and 3 list the predicted ultimate bond strength, $P_{u,pre}$, and predicted effective bond lengths, $L_{e,pre}$, for experimental and numerical specimens, respectively. The ratios, $P_{u,pre}/\bar{P}_{u,exp}$, in Table 2 and the ratios, $P_{u,pre}/P_{u,num}$, in Table 3 are between 0.91 and 1.10 for three-layered hybrid FRP-to-steel single-lap joints. It indicates that the experimental and numerical ultimate bond strength can be accurately predicted when $E_f t_f$ is determined by Eq. (6). In Tables 2 and 3, the predicted effective bond lengths are also in good agreement with the experimental and numerical results. Remarkably, in Table 2, the predicted effective bond length of three-layered hybrid FRP-to-steel single-lap joints is close to that of three-layered CFRP-to-steel single-lap joints ($23.6/27.8 \approx 0.85$), which is consistent with the test observation. Therefore, the modified equation for the axial stiffness of the hybrid FRP can reflect the influence of the hybrid effect between the inner and outer layers of GFRP and the intermediate layer of CFRP on the ultimate bond strength and effective bond lengths of three-layered hybrid FRP-to-steel joints.

5. Conclusions

This paper presents experimental and numerical studies on the bond behavior of three-layered hybrid FRP-to-steel single-lap joints. Experimental results show that there is a possible hybrid effect between the inner and outer layers of GFRP and the intermediate layer of CFRP. Then, the numerical investigation further confirms the hybrid effect. Finally, a modified equation for the axial stiffness of the hybrid FRP is proposed to consider the influence of the hybrid effect on the ultimate bond strength and effective bond lengths of hybrid FRP-to-steel joints. The following conclusions can be drawn from the presented work:

(1) Three-layered hybrid FRP-to-steel joints have similar failure modes with three-layered CFRP-to-steel joints. Cohesive failure (M2) occurs when the bond length is 20 mm, while both cohesive failure (M2) and FRP delamination (M4) occur when the bond length

Table 3
Numerical and predicted results.

No.	Inner and outer layers of GFRP			Intermediate layer of CFRP			Numerical results		Predicted results			
	E_{gf} (GPa)	t_{gf} (mm)	$E_{gf}t_{gf}$ (GPa·mm)	E_{cf} (GPa)	t_{cf} (mm)	$E_{cf}t_{cf}$ (GPa·mm)	P_{num} (kN)	$L_{e,num}$ (mm)	$P_{u,pre}$ (kN)	$\frac{P_{u,pre}}{P_{u,num}}$	$L_{e,pre}$ (mm)	Y/N[f]
HFa-20	64.0[a]	0.240[a]	15.36	236.7	0.167	39.53	2.69	20 ~ 30	–	–	21.2	Y
HFa-40							3.67		3.59	0.98		
HFa-60							3.69		3.59	0.97		
HFa-80							3.82		3.59	0.94		
HF-20	76.0	0.340	25.84	236.7	0.167	39.53	2.89	20 ~ 30	–	–	23.6	Y
HF-40							4.02		3.98	0.99		
HF-60							4.13		3.98	0.96		
HF-80							4.21		3.98	0.95		
HFb-20	93.1[b]	0.338[b]	31.47	236.7	0.167	39.53	2.90	20 ~ 30	–	–	24.2	Y
HFb-40							4.16		4.09	0.98		
HFb-60							4.29		4.09	0.95		
HFb-80							4.33		4.09	0.94		
HFc-20	73.0[c]	0.540[c]	39.42	236.7	0.167	39.53	3.04	20 ~ 30	–	–	26.9	Y
HFc-40							4.22		4.54	1.08		
HFc-60							4.30		4.54	1.06		
HFc-80							4.47		4.54	1.02		
HFd-20	76.0	0.340	25.84	252.0[d]	0.111[d]	27.97	2.61	20 ~ 30	–	–	22.2	Y
HFd-40							3.39		3.74	1.10		
HFd-60							3.52		3.74	1.06		
HFd-80							3.61		3.74	1.04		
HFe-20	76.0	0.340	25.84	206.6[e]	0.176[e]	36.36	2.57	20 ~ 30	–	–	22.7	Y
HFe-40							3.61		3.84	1.06		
HFe-60							3.78		3.84	1.01		
HFe-80							3.89		3.84	0.98		

Note: [a], [b], [c], [d] and [e] represent that the properties of FRP were from [42–45] and [32], respectively.
[f]Y and N represent the predicted effective bond length agrees and does not agree with the numerical result, respectively.

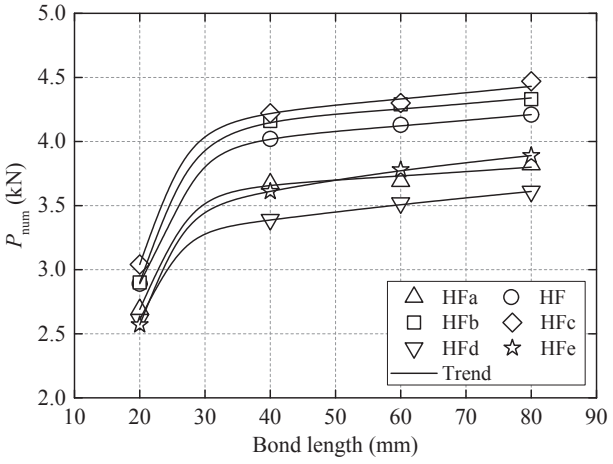

Fig. 8. Numerical bond strength versus bond length relationships.

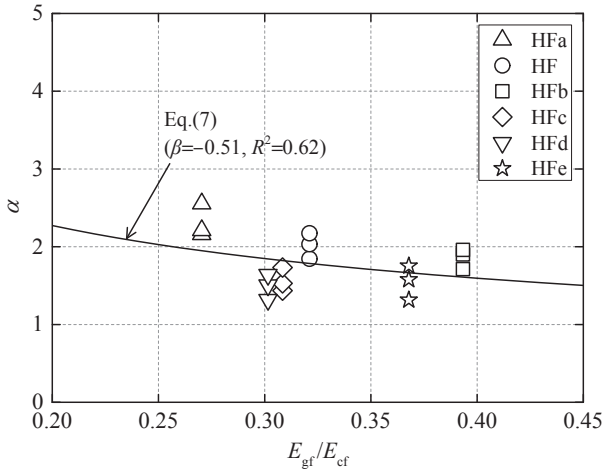

Fig. 9. Regression analysis for the determination of β.

exceeds 40 mm.

(2) The bond strength of three-layered hybrid FRP-to-steel joints greatly increases compared to that of one-layered CFRP-to-steel joints. From three-layered hybrid FRP-to-steel joints to three-layered CFRP-to-steel joints, the reduction of the bond strength is slight.
(3) The effective bond length of three-layered hybrid FRP-to-steel joints is greater than that of one-layered CFRP-to-steel joints but close to that of three-layered CFRP-to-steel joints.
(4) The numerical investigation shows that each layer of FRP in the three-layered hybrid FRP-to-steel joint undergoes greater deformation than the corresponding layer of FRP in the three-layered CFRP-to-steel joint during loading. It confirms that a hybrid effect exists between the inner and outer layers of GFRP and the intermediate layer of CFRP. This is the reason for the effective use of the hybrid FRP to strengthen steel structures.
(5) Taking into account the hybrid effect between GFRP and CFRP, a modified equation is proposed to determine the axial stiffness of the hybrid FRP. Base on this modification and existing models for CFRP-to-steel joints, the ultimate bond strength and effective bond lengths of hybrid FRP-to-steel joints can be predicted.

CRediT authorship contribution statement

Bo Hu: Conceptualization, Methodology, Writing - review & editing, Supervision. **Yuan Li:** Software, Validation, Writing - original draft. **Yu-Tian Jiang:** Data curation, Writing - original draft. **Huai-Zhong Tang:** Resources, Investigation.

Declaration of Competing Interest

The authors declare that they have no known competing financial interests or personal relationships that could have appeared to

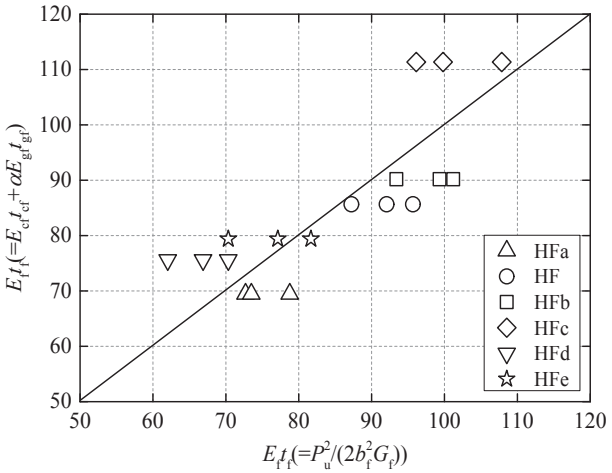

Fig. 10. Comparison between $E_f t_f$ calculated by Eq. (6) and $E_f t_f$ back-calculated by Eq. (8).

influence the work reported in this paper.

Acknowledgments

This work was supported by the National Natural Science Foundation of China under Grant No. 51408175. The authors wish to thank Dr. Yun-Lin Liu from Anhui Jianzhu University, Dr. Jun-Qi Huang from The Hong Kong Polytechnic University and Mr. Teng-Fei Meng from Hefei University of Technology for their assistance during the test program.

Data availability

All relevant data are included within the paper.

Appendix A. Supplementary data

Supplementary data to this article can be found online at https://doi.org/10.1016/j.compstruct.2020.111936.

References

[1] Zhao XL, Zhang L. State-of-the-art review on FRP strengthened steel structures. Eng Struct 2007;29(8):1808–23.
[2] Teng JG, Yu T, Fernando D. Strengthening of steel structures with fiber-reinforced polymer composites. J Constr Steel Res 2012;78(11):131–43.
[3] Hosseini A, Ghafoori E, Al-Mahaidi R, Zhao XL, Motavalli M. Strengthening of a 19th-century roadway metallic bridge using nonprestressed bonded and prestressed unbonded CFRP plates. Constr Build Mater 2019;209:240–59.
[4] Haghani R, Al-Emrani M. A new design model for adhesive joints used to bond FRP laminates to steel beams - Part B: Experimental verification. Constr Build Mater 2012;30:686–94.
[5] Shaat A, Fam A. Axial loading tests on short and long hollow structural steel columns retrofitted using carbon fibre reinforced polymers. Can J Civ Eng 2006;33(4):458–70.
[6] Harries KA, Peck AJ, Abraham EJ. Enhancing stability of structural steel sections using FRP. Thin-Walled Struct 2009;47(10):1092–101.
[7] Hosseini A, Ghafoori E, Motavalli M, Nussbaumer A, Zhao XL. Mode I fatigue crack arrest in tensile steel members using prestressed CFRP plates. Compos Struct 2017;178:119–34.
[8] Hosseini A, Ghafoori E, Motavalli M, Nussbaumer A, Zhao XL, Al-Mahaidi R, et al. Development of prestressed unbonded and bonded CFRP strengthening solutions for tensile metallic members. Eng Struct 2019;181:550–61.
[9] Shamsuddoha M, Islam MM, Aravinthan T, Manalo A, Lau K. Effectiveness of using fibre-reinforced polymer composites for underwater steel pipeline repairs. Compos Struct 2013;100:40–54.
[10] Tavakkolizadeh M, Saadatmanesh H. Galvanic corrosion of carbon and steel in aggressive environments. J Compos Constr 2001;5(3):200–10.
[11] Hollaway LC, Cadei J. Progress in the technique of upgrading metallic structures with advanced polymer composites. Prog Struct Mat Eng 2002;4(2):131–48.
[12] Alexander C. Development of a composite repair system for reinforcing offshore risers PhD thesis Texas: Texas: A&M University; 2007.
[13] Photiou NK, Hollaway LC, Chryssanthopoulos MK. Strengthening of an artificially degraded steel beam utilising a carbon/glass composite system. Constr Build Mater 2006;20(1–2):11–21.
[14] Sweedan AMI, Alhadid MMA, El-Sawy KM. Experimental study of the flexural response of steel beams strengthened with anchored hybrid composites. Thin-Walled Struct 2016;99:1–11.
[15] Xia SH, Teng JG. Behaviour of FRP-to-steel bonded joints. Proceedings of the International Symposium on Bond Behavior of FRP in Structures. Hong Kong: International Institute for FRP in Construction; 2005. p. 411–8.
[16] Akbar I, Oehlers DJ, Mohamed Ali MS. Derivation of the bond-slip characteristics for FRP plated steel members. J Constr Steel Res 2010;66(8–9):1047–56.
[17] Yu T, Fernando D, Teng JG, Zhao XL. Experimental study on CFRP-to-steel bonded interfaces. Compos B Eng 2012;43(5):2279–89.
[18] Fawzia S. Evaluation of shear stress and slip relationship of composite lap joints. Compos Struct 2013;100:548–53.
[19] He J, Xian G. Debonding of CFRP-to-steel joints with CFRP delamination. Compos Struct 2016;153:12–20.
[20] Wang HT, Wu G, Dai YT, He XY. Determination of the bond-slip behavior of CFRP-to-steel bonded interfaces using digital image correlation. J Reinf Plast Compos 2016;35:1353–67.
[21] Wang HT, Wu G, Dai YT, He XY. Experimental study on bond behavior between CFRP plates and steel substrates using digital image correlation. J Compos Constr 2016;20(6):04016054.
[22] Hosseini A, Ghafoori E, Wellauer M, Marzaleh AS, Motavalli M. Short-term bond behavior and debonding capacity of prestressed CFRP composites to steel substrate. Eng Struct 2018;176:935–47.
[23] Martinelli E, Hosseini A, Ghafoori E, Motavalli M. Behavior of prestressed CFRP plates bonded to steel substrate: Numerical modeling and experimental validation. Compos Struct 2019;207:974–84.
[24] Colombi P, Poggi C. Strengthening of tensile steel members and bolted joints using adhesively bonded CFRP plates. Constr Build Mater 2006;20(1–2):22–33.
[25] Fawzia S, Al-Mahaidi R, Zhao XL. Experimental and finite element analysis of a double strap joint between steel plates and normal modulus CFRP. Compos Struct 2006;75(1–4):156–62.
[26] Bocciarelli M, Colombi P, Fava G, Poggi C. Interaction of interface delamination and plasticity in tensile steel members reinforced by CFRP plates. Int J Fract 2007;146(1):79–92.
[27] Bocciarelli M, Colombi P, Fava G, Poggi C. Prediction of debonding strength of tensile steel/CFRP joints using fracture mechanics and stress based criteria. Eng Fract Mech 2009;76(2):299–313.
[28] Fawzia S, Zhao XL, Al-Mahaidi R. Bond-slip models for double strap joints strengthened by CFRP. Compos Struct 2010;92(9):2137–45.
[29] Chiew SP, Yu Y, Lee CK. Bond failure of steel beams strengthened with FRP laminates - Part 1: Model development. Compos B Eng 2011;42(5):1114–21.
[30] Al-Zubaidy H, Al-Mahaidi R, Zhao XL. Experimental investigation of bond characteristics between CFRP fabrics and steel plate joints under impact tensile loads. Compos Struct 2012;94(2):510–8.
[31] Wu C, Zhao XL, Hui Duan W, Al-Mahaidi R. Bond characteristics between ultra high modulus CFRP laminates and steel. Thin-Walled Struct 2012;51(2):147–57.
[32] Al-Zubaidy H, Al-Mahaidi R, Zhao XL. Finite element modelling of CFRP/steel double strap joints subjected to dynamic tensile loadings. Compos Struct 2013;99:48–61.
[33] Al-Mosawe A, Al-Mahaidi R, Zhao XL. Effect of CFRP properties on the bond characteristics between steel and CFRP laminate under quasi-static loading. Constr Build Mater 2015;98:489–501.
[34] Korayem AH, Li CY, Zhang QH, Zhao XL, Duan WH. Effect of carbon nanotube modified epoxy adhesive on CFRP-to-steel interface. Compos B Eng 2015;79:95–104.
[35] Yang Y, Biscaia H, Chastre C, Silva MAG. Bond characteristics of CFRP-to-steel joints. J Constr Steel Res 2017;138:401–19.
[36] Hai ND, Mutsuyoshi H. Structural behavior of double-lap joints of steel splice plates bolted/bonded to pultruded hybrid CFRP/GFRP laminates. Constr Build Mater 2012;30(5):347–59.
[37] GB/T 700-2006. Carbon structural steels. Chinese Standard, Standardization Administration of the People's Republic of China, China; 2006. (in Chinese).
[38] GB/T228.1-2010. Metallic materials-Tensile testing-Part 1: Method of test at room temperature. Chinese Standard, Standardization Administration of the People's Republic of China, China; 2010. (in Chinese).
[39] YB/T 4558-2016. Technical specification for strengthening steel structures with fiber reinforced polymer. Chinese Standard, Ministry of Industry and Information Technology of the People's Republic of China, China; 2010. (in Chinese).
[40] Wu Z, Yuan H, Niu H. Stress transfer and fracture propagation in different kinds of adhesive joints. J Eng Mech 2002;128(5):562–73.
[41] ABAQUS. ABAQUS 6.13 Documentation. Dessault systems; 2013.
[42] Capozucca R. Vibration analysis of damaged RC beams strengthened with GFRP. Compos Struct 2018;200:624–34.
[43] Weng D, Lu X, Zhou C, Kubo T, Li K. Experimental study on seismic retrofitting of masonry walls using GFRP. 13th World Conference on Earthquake Engineering, Vancouver, 2006, Paper No. 1981.
[44] Dong JF, Wang QY, Guan ZW. Structural behavior of RC beams externally strengthened with FRP sheets under fatigue and monotonic loading. Eng Struct 2012;41:24–33.
[45] Li S, Zhu T, Lu Y, Lu YY, Li XJ. Effect of temperature variation on bond characteristics between CFRP and steel plate. Int J Polymer Sci 2016;1:1–8.